JMEPEG (2012) 21:1232–1242
DOI: 10.1007/s11665-011-0037-7

1059-9495/$19.00

Transient Liquid-Phase Diffusion Bonding of Aluminum Metal Matrix Composite Using a Mixed Cu-Ni Powder Interlayer

Joydeep Maity and Tapan Kumar Pal

(Submitted May 12, 2011)

In the present study, the transient liquid-phase diffusion bonding of an aluminum metal matrix composite (6061-15 wt.% SiCp) has been investigated for the first time using a mixed Cu-Ni powder interlayer at 560 °C, 0.2 MPa, for different holding times up to 6 h. The microstructure of the isothermally solidified zone contains equilibrium precipitate $CuAl_2$, metastable precipitate Al_9Ni_2 in the matrix of α-solid solution along with the reinforcement particles (SiC). On the other hand, the microstructure of the central bond zone consists of equilibrium phases such as $NiAl_3$, Al_7Cu_4Ni and α-solid solution along with SiC particles (without any segregation) and the presence of microporosities. During shear test, the crack originates from microporosities and propagates along the interphase interfaces resulting in poor bond strength for lower holding times. As the bonding time increases, with continual diffusion, the structural heterogeneity is diminished, and the microporosities are eliminated at the central bond zone. Accordingly, after 6-h holding, the microstructure of the central bond zone mainly consists of $NiAl_3$ without any visible microporosity. This provides a joint efficiency of 84% with failure primarily occurring through decohesion at the SiC particle/matrix interface.

Keywords 6061-SiCp composite, Cu-Ni powder interlayer, joint efficiency, joint microstructure, transient liquid-phase diffusion bonding

1. Introduction

The development of various metal matrix composites (MMCs) is regarded as a major advancement in materials science and technology during the past few decades. The silicon carbide (SiC)-reinforced aluminum-based metal matrix composites (AlMMCs) exhibit better properties as compared to the monolithic aluminum alloys which make these composites useful for aerospace and transportation industry applications (Ref 1, 2). Despite the potential advantages of using AlMMCs, they have not reached widespread industrial applications. One of the main reasons of the limited use of AlMMCs is the difficulty encountered in their joining (Ref 3). Mechanical fastening (bolting or riveting) involves drilling the composite, which would cause damage to the reinforcement as well as creating stress concentrations leading to catastrophic failure (Ref 4). Fusion welding of SiC-reinforced AlMMC is associated with number of difficulties, such as high viscosity of melt, segregation effects on re-solidification, evolution of occluded gases causing extensive cracking in the heat affected zone and weld porosity, and particle/matrix reaction producing detrimental intermetallic compound (Al_4C_3). The presence of Al_4C_3 platelets reduces fracture toughness of weld and causes corrosion in moist environment (Ref 5–7). The main problem associated with solid-state diffusion bonding of AlMMC is the presence of tenacious and stable aluminum oxide layer at surface that inhibits metal-to-metal contact (Ref 8). To overcome this difficulty, application of high pressure is required, which causes a plastic deformation in excess of 40% to disrupt oxide film on faying surfaces (Ref 9). Other alternative is the removal of oxide layer before bonding by ion-beam cleaning in vacuum. Both these approaches are difficult to practice in industrial applications (Ref 10).

The transient liquid-phase (TLP) diffusion bonding process has been reported as a promising technique by several investigators for joining the AlMMCs (Ref 10–13). The TLP diffusion bonding process is an intriguing approach of joining which applies an interlayer between the pieces to be joined where the interdiffusion of the interlayer and the base material leads to the formation of a low-melting composition (eutectic) that melts, widens, shrinks, and solidifies at a fixed bonding temperature. The process has advantages of a low bonding temperature, low bonding pressure, the absence of a heat-affected zone, disruption of the surface oxide film by the TLP, and a low probability of unfavorable reaction (Ref 10, 14–16). The TLP diffusion bonding process was first introduced and patented by Paulonis et al. in the year 1972, in the US (Ref 17). During that period, the process was introduced for joining the heat-resistant alloys, such as nickel-based superalloys (Ref 14). Later on, along with the nickel-based superalloys [inconel, oxide dispersion-strengthened (ODS) nickel alloy, etc.] (Ref 18, 19), it has been also applied to other materials such as

Joydeep Maity, Department of Metallurgical and Materials Engineering, National Institute of Technology, Durgapur 713209 West Bengal, India; and **TapanKumar Pal**, Welding Technology Center, Department of Metallurgical and Material Engineering, Jadavpur University, Kolkata 700032 West Bengal, India. Contact e-mails: joydeep_maity@yahoo.co.in and tkpal.ju@gmail.com.

magnesium alloys (Ref 20), duplex stainless steel (Ref 21, 22), titanium aluminide (Ref 23), dissimilar material joining (ODS ferritic steel to silicon nitride) (Ref 24), and MMCs (Ref 10–13, 25–27).

In the TLP process, the bonding temperature is kept slightly above the eutectic temperature of the interlayer-base material system and below the solidus temperature of the base material. The most widely used interlayer in TLP diffusion bonding of AlMMCs is the Cu since it involves a low bonding temperature (the eutectic temperature of the Al-Cu system is 548 °C) which is considerably far below the solidus temperature of base material to prevent melting or distortion. The initial attempts by Bushby and Scott (Ref 25, 26) to join a SiC fiber-reinforced AlMMC with Cu foil and Ag-Cu foil interlayer at 550 °C in air environment, resulted in a poor joint strength because of the oxidation of transient liquid. Klehn and Eagar (Ref 27) achieved better joint efficiency during the TLP diffusion bonding of 6061-15 vol.% Al_2O_3 in vacuum with Cu-foil and Ag-foil interlayers. Although the different stages of the TLP bonding process were not studied for composite system, the segregation of Al_2O_3 reinforcement at the bond interface was reported up to a maximum holding time of 2 h at 566 °C. In general, particle segregation (agglomeration) at the bond region has been observed during the TLP diffusion bonding of AlMMCs containing alumina and SiC-particle-reinforced Cu, and when joining yttria-bearing ODS alloys. In particular, for the TLP bonding of SiC- or Al_2O_3-reinforced AlMMCs, the use of pure copper interlayer causes reinforcement particle segregation at the bond interface (Ref 28, 29). The region of weakness produced by the particle segregation at the bond region has been found to promote preferential failure during tensile testing (Ref 28). On the other hand, the use of pure nickel interlayer has shown no disruption of particle reinforcement dispersion (Ref 30), but the bonding temperature usually exceeds 650 °C (since the Al-Ni eutectic temperature is 640 °C), which is above or close to the solidus temperature of most aluminum matrix alloys, causing melting or great deal of distortion of the base material and joining becomes impossible. Yan et al. (Ref 13) used a Cu/Ni/Cu composite foil interlayer (instead of pure Cu or pure Ni) of thickness 10/30/10-μm for joining 6061-30 vol.% Al_2O_3 composite by the TLP diffusion bonding process at 580 °C (just below the solidus temperature of 6061 alloy, 582 °C (Ref 31)) with 30-90-min holding time in vacuum (pressure not mentioned). The maximum bond strength of 102 MPa was achieved for the highest bonding time (90 min) used, which is 68% of the parent composite strength (150 MPa). The use of composite foil interlayer produced a highly heterogeneous-layered microstructure along with the presence of intermetallic brittle phase $Al_{0.9}Ni_{1.1}$ that hindered obtaining adequate joint efficiency. However, the use of uniformly mixed Cu-Ni powder interlayer has not been studied so far for joining AlMMCs by the TLP diffusion bonding process. Therefore, in the present research study, a mixed Cu-Ni powder interlayer is thought of as the one that would provide more uniformity in microstructure with the progress of diffusion during the TLP process. Accordingly, the 6061-15 wt.% SiCp composite is bonded with mixed Cu-Ni powder interlayer (1:1 proportion by weight) in an argon environment with different holding times up to 6 h. The microstructural evolution with bonding time has been thoroughly investigated in correlation with the joint shear strength and the mode of failure.

2. Experimental Procedure

2.1 Material

The as-received material for the TLP diffusion bonding was an extruded rod of AlMMC consisting of 6061 matrix alloy (1.0 wt.% Mg, 0.6 wt.% Si, 0.3 wt.% Cu, 0.2 wt.% Cr, 0.6 wt.% Fe and balance Al) and 15 wt.% (13 vol.%) silicon carbide (SiC) particulate reinforcement. The material was supplied by the Regional Research Laboratory, Thiruvananthapuram, India, in the form of a cast billet with average size of SiC particles being 23 μm. The cast billet was then extruded at the National Metallurgical Laboratory, Jamshedpur, India, into a rod at 415 °C temperature with an extrusion ratio of 20:1.

2.2 Specimen Preparation and TLP Diffusion Bonding

The extruded rod was machined to produce disks of 15 mm in diameter and 10 mm in height. The faying surfaces of the disks were polished at first with different grades of emery papers soaked in kerosene and liquid paraffin (1:1 proportion) up to 1000 grit, and finally with 1 μm diamond paste. Thereafter, the surfaces were rinsed in acetone and dried by hot air blast. In order to maintain a mixed interlayer of copper powder and nickel powders (1:1 proportion by weight) of 50-μm thickness, initially a total mass of 82 mg powder (41 mg each of the copper powder and the nickel powder) was taken and thoroughly mixed. After applying the powder mixture between the disks, the assembly was pressed from both sides and set by an adhesive tape. During compaction (while pressing the assembly from both sides), some amounts of powder was lost from the peripheral region of the cross section. Then, the tape was locally dislodged at the joint region, and the thickness of the powder interlayer was measured under optical microscope with graduated eye piece. The thickness of 50 μm was fixed on several trials. Thereafter, the weight gain of the assembly was measured in a digital microbalance (PRECISA-

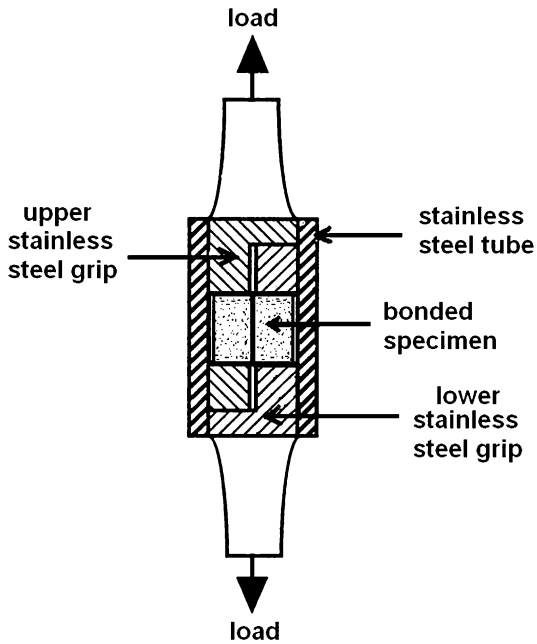

Fig. 1 Specimen loaded in jig: the arrangement for shear strength (bond strength) determination

205A-SCS, Switzerland) to determine the actual mass of the powder interlayer. Considering all the specimens, the mass of mixed powder interlayer (in terms of mean ± standard deviation) was found to be 74 ± 2 mg. The assembly was then inserted inside the diffusion bonding unit (programmable electric furnace), where the bonding was carried out at 560 °C under 0.2 MPa pressure in an argon environment. A thermocouple inserted into the drilled hole in one of each pair of disks was used for monitoring the bonding temperature. The bonding temperature (560 °C) was kept above the eutectic temperature (548 °C) of the Al-Cu system (Ref 32) and below the solidus temperature (582 °C) of 6061 matrix alloy (Ref 31). The specimens were heated to the bonding temperature at a rate of 6 °C/min, held at that temperature for five different lengths of time (bonding time)—40 min, 1 h, 2 h, 3 h and 6 h—and cooled down to 540 °C at a rate of 5 °C/min inside the furnace. The specimens were subsequently taken out of the furnace and allowed to air-cool.

2.3 Mechanical Testing

Bonded cylindrical samples were machined to 10-mm diameter to eliminate edge effects. These specimens (bonded composites) of approximately 20-mm length and 10-mm diameter and the as-received composite of similar dimension were loaded in a specially prepared jig, which is schematically shown in Fig. 1. The grips of the jig were pulled in tension in a 100 KN capacity universal testing machine (INSTRON-8862) at a cross head speed of 0.5 mm/min in position control mode such that the specimen experienced pure shear stress across the bond interface. The maximum load was divided by the bond area to calculate shear strength. For each bonding condition, three specimens were tested, and the mean value along with

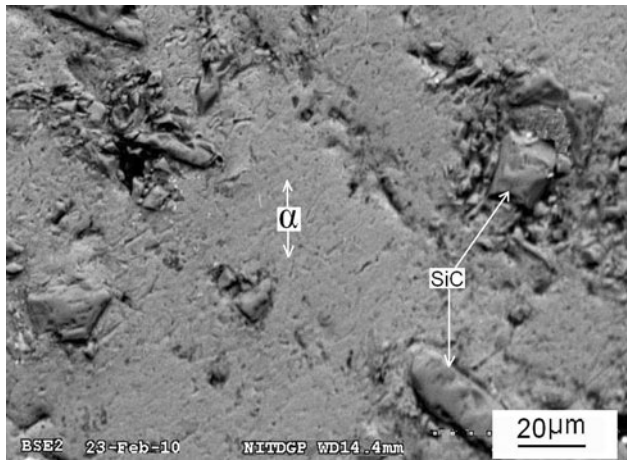

Fig. 2 Back-scattered electron image of the polished section of as-received 6061-SiCp composite

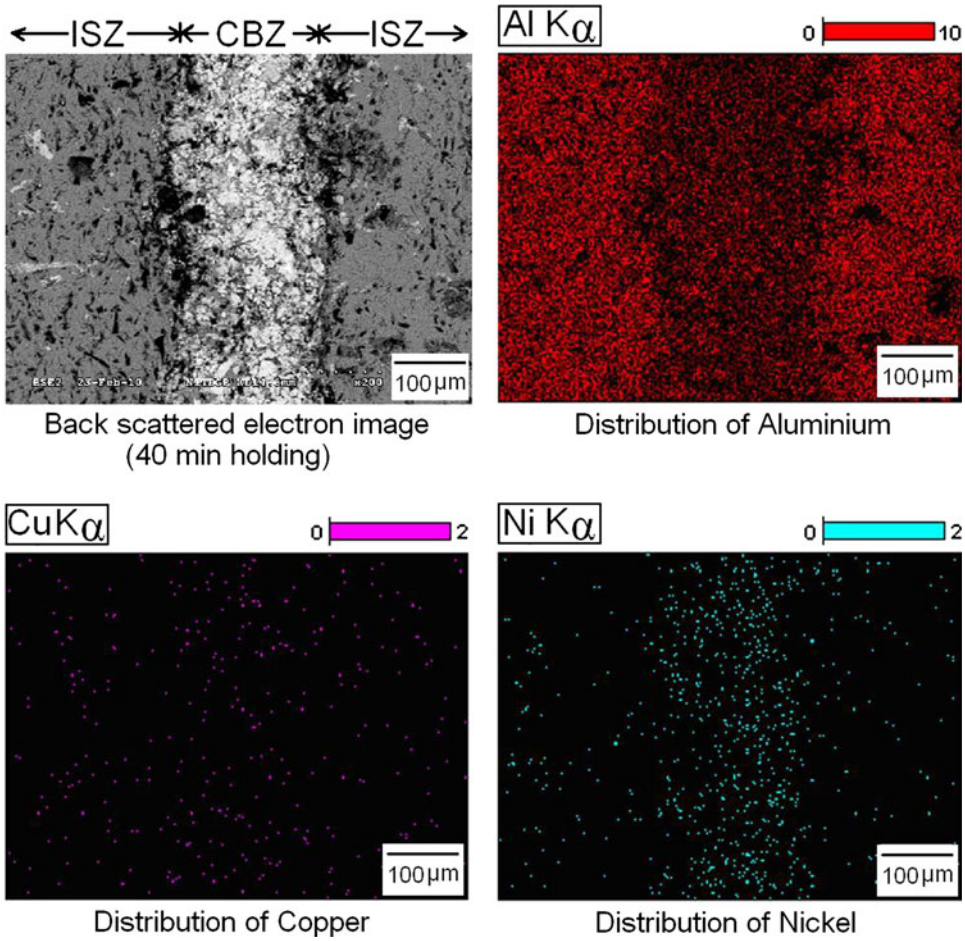

Fig. 3 Back-scattered electron image and elemental distribution of the polished and etched section representing the entire bond region for 40-min holding

Table 1 Calculation of diffusivity for Cu and Ni

Diffusing species	Matrix	Frequency factor (D_0), m^2/s	Activation energy (Q), J/mol	Temperature (T), K	Diffusivity (D), m^2/s
Cu	Al	1.50×10^{-5}	1.26×10^5	833	1.89×10^{-13}
Ni	Al	1.87×10^{-4}	2.68×10^5	833	2.92×10^{-21}

standard deviation is considered as the shear strength (bond strength). The procedure followed for shear strength's determination is in accordance with the standard procedure considered by most of the investigators (Ref 10–13, 29) in the field of TLP diffusion bonding.

2.4 Scanning Electron Microscopy and Energy Dispersive X-Ray Spectroscopy

The bonded cylindrical samples were sectioned perpendicular to the bonding plane. The section was polished at first with different grades of emery papers soaked in kerosene and liquid paraffin (1:1 proportion) up to 1000 grit, and finally with 1 μm diamond paste. Thereafter, these were mildly etched with Keller's reagent. The bond region of these metallographic specimens and the fractured surfaces of the shear-tested specimens were examined under a scanning electron microscope (Hitachi, S-3000N, Japan). Reasonable phase contrast was achieved in the back-scattered electron image mode. Different phases were identified by the spot analysis using Energy Dispersive X-ray Spectroscopy (EDS) with built-in ZAF correction. For a particular phase, the data of 10 spots were taken into consideration, and the phase was identified by the calculated mean and standard deviation values of the at.% of the elements present. Furthermore, the distribution of different elements in the bond region was studied by elemental mapping. Thereafter, the vol.% of different phases present in the central bond zone was determined using graphical point count method onto the SEM back-scattered electron micrographs. During point counting, 10 image frames were considered for each bonding condition, and the average value is reported.

2.5 X-Ray Diffraction Study

In order to further identify the different phases present, thin specimens were machined out from the bond region and were subjected to X-ray diffraction (XRD) analysis at extremely slow scan rate (0.5^0/min) in a high resolution X-ray diffractometer (Regaku Miniflex, Japan).

3. Results and Discussion

3.1 Microstructural Evaluation

The back-scattered electron image (Fig. 2) of the as-received composite exhibits the presence of SiC particles in the 6061 aluminum alloy matrix. The back-scattered electron image of the bonded specimen with 40-min holding, representing the overall view of the bond region at low magnification along with the distribution of different significant elements (elemental mapping), is presented in Fig. 3. The atomic number contrast in the back-scattered electron image mode indicates the presence of two zones at the bond region, namely (i) central bond zone (indicated as "CBZ"), and (ii) isothermally solidified zone (indicated as "ISZ"). The CBZ is the zone just around the bond

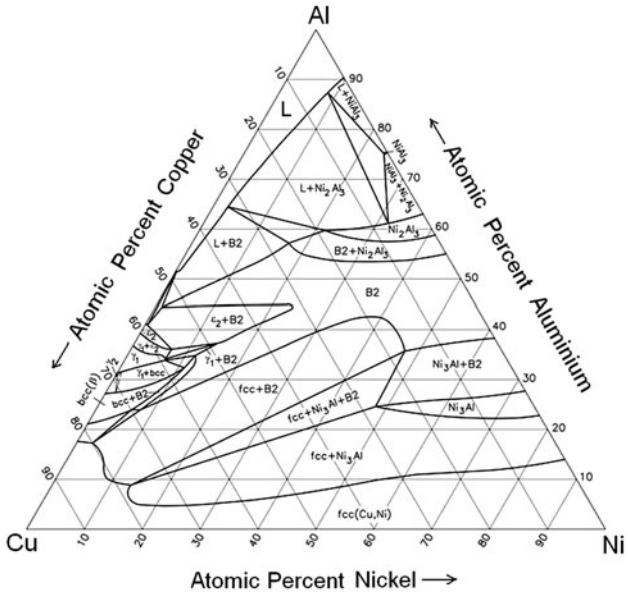

Fig. 4 Al-Cu-Ni ternary phase diagram at 800 °C (after Ref 34)

centerline, and being enriched with high atomic number interlayer elements (Cu and Ni), it possesses an overall bright appearance. The adjacent regions on both sides (ISZ) is relatively dull in appearance due to the abundance of aluminum (element of low atomic number). The elemental maps indicate that the distribution of Cu is more uniform than Ni. Copper is almost evenly distributed in CBZ and ISZ. However, although Ni is present both in CBZ and ISZ, it is more concentrated in CBZ. Table 1 shows the calculation of the diffusivity (D) of Cu in Al and that of Ni in Al at the bonding temperature (T = 833 K) based on the values of the frequency factor (D_0) and the activation energy (Q) obtained from the standard literature (Ref 16, 33) using the relationship: $D = D_0\ e^{-Q/RT}$ (where, R = 8.314 J/mol/K, the molar gas constant). It is found that at 560 °C, the diffusivity of Cu is about 10^8 times higher than that of Ni. Thus, the interlayer material Cu diffuses readily to the adjacent region away from the bond centerline. On the other hand, Ni exhibits a limited diffusion. On heating to the bonding temperature (560 °C) at a rate 6 °C/min and holding at this temperature for 40 min, Ni has only diffused to a thickness of about 100 μm (Fig. 3) from an initial interlayer thickness of 50 μm; whereas Cu is found to be distributed in a much wider region (more than 500 μm). In fact, during holding at the bonding temperature, the interdiffusion of three major elements, viz., Cu, Ni (present in the powder interlayer), and Al (present in 6061 matrix alloy), determines the microstructure of the joint region. The melting points of Ni, Cu, and Al are 1453, 1083, and 660 °C, respectively. The liquidus line of Cu-Ni binary isomorphous system and the eutectic temperature of Al-Ni binary system (640 °C) are much higher than the bonding

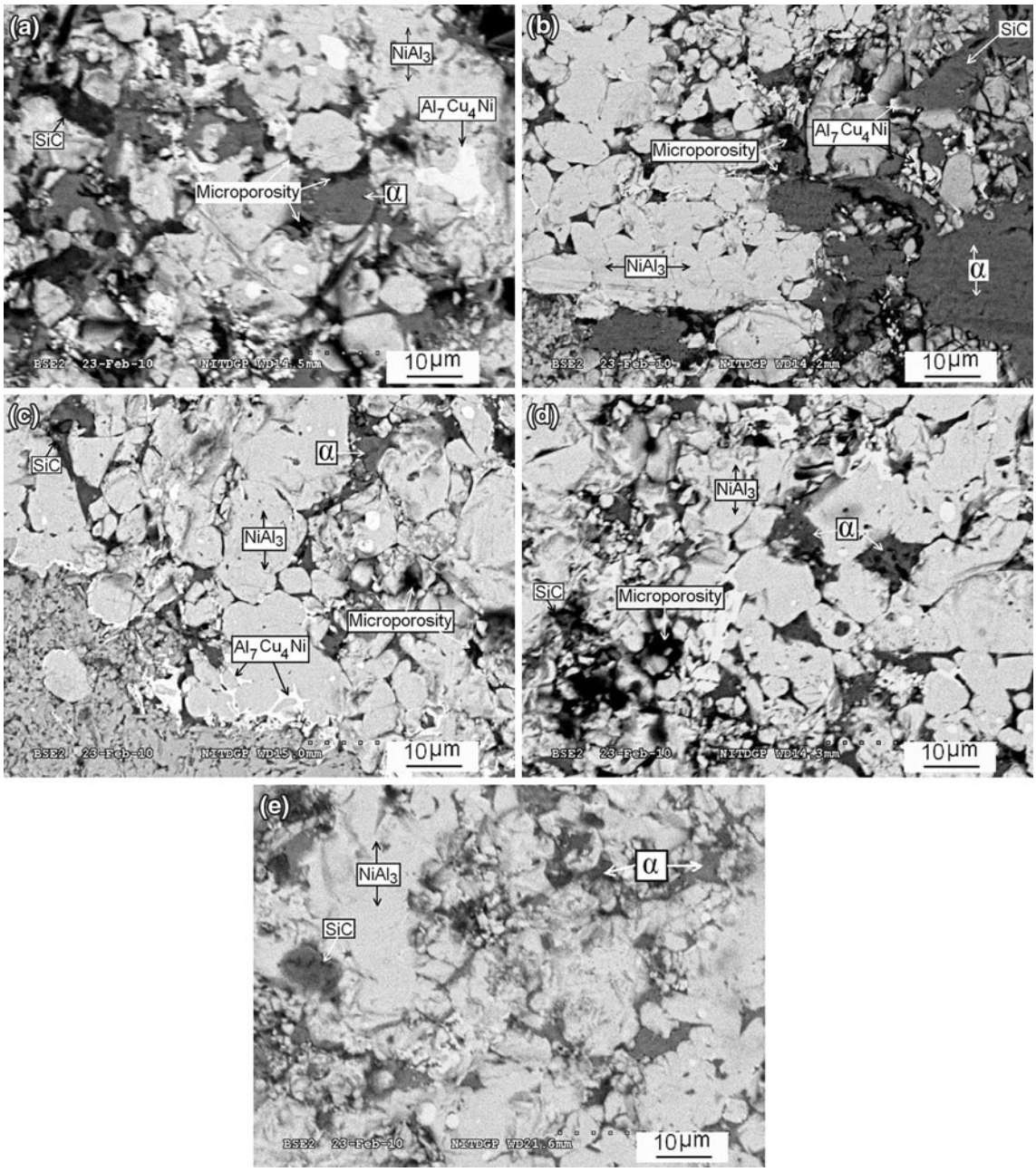

Fig. 5 Back-scattered electron images of the polished and etched section representing central bond zone for different holding times: (a) 40 min, (b) 1 h, (c) 2 h, (d) 3 h, and (e) 6 h

Table 2 Result of point count analysis at central bond zone

Bonding time	% $NiAl_3$	% α-solid solution	% Al_7Cu_4Ni	% SiC	% Porosity
40 min	62.66	16.03	10.02	2.25	9.04
1 h	63.45	16.39	8.89	2.34	8.93
2 h	76.81	10.51	4.55	2.12	6.01
3 h	82.01	10.62	Absent	2.03	5.34
6 h	87.68	10.11	Absent	2.21	Absent

temperature (560 °C). However, the eutectic temperature of Al-Cu binary system (548 °C) is lower than the bonding temperature (Ref 32). A complete ternary phase diagram of Al-Cu-Ni system near the bonding temperature (560 °C) is not readily available in the literature. However, it is available at relatively higher temperature (Ref 34) as shown in Fig. 4. A

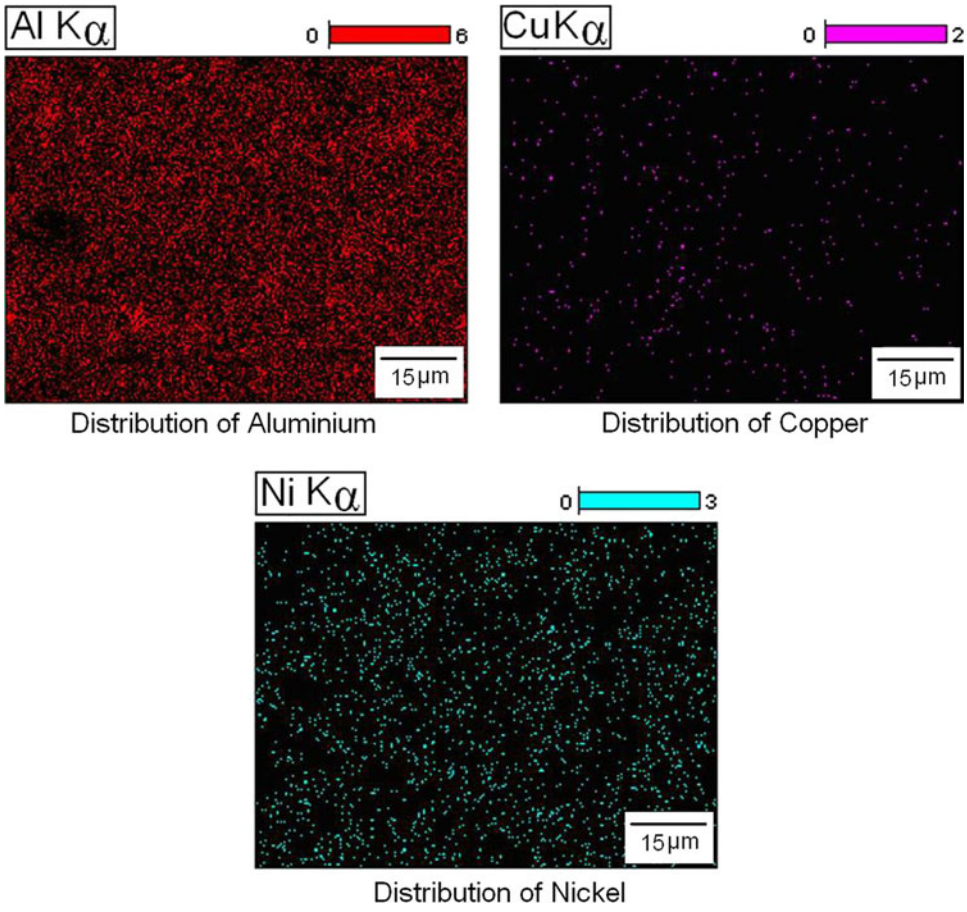

Fig. 6 The elemental distribution at the central bond zone for a bonding time of 6 h (corresponding to Fig. 5e)

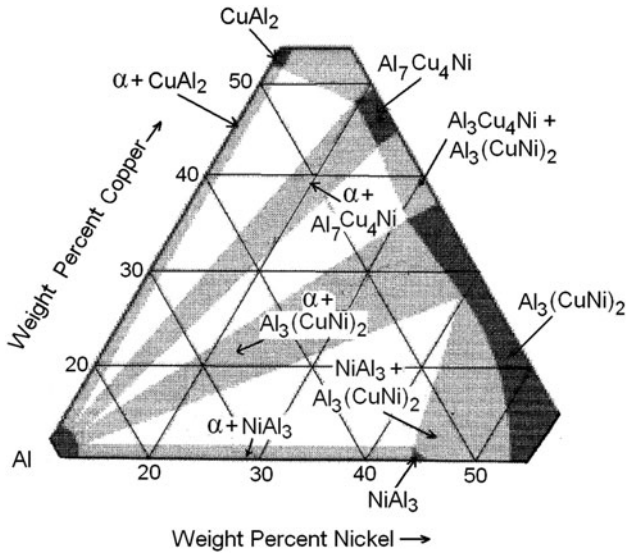

Fig. 7 Al-Cu-Ni ternary phase diagram at room temperature (after Ref 36)

stable liquid phase is found in the Al-Cu-enriched part; on the other hand, Ni-enriched part consists of several phases at the solid state. Therefore, during holding of the assembly at the bonding temperature, the interlayer melting is likely to start preferably at the interlayer-base material interface, and the molten zone (liquid) is likely to expand toward the base material through faster diffusion of copper into the aluminum alloy matrix. This molten zone is likely to undergo isothermal solidification generating ISZ. On the other hand, the region just around the bond centerline (CBZ), being enriched with Ni (due to lower diffusivity of Ni), is likely to undergo partial melting. The melting would occur in the local region concentrated with Al and Cu; on the other hand, the Ni-enriched region will undergo phase transformation through solid-state diffusion. Therefore, a considerable structural heterogeneity is expected in CBZ. The back-scattered electron images of CBZ at higher magnification are presented in Fig. 5a-e. The specimen with 40-min holding time (Fig. 5a) exhibits a highly heterogeneous microstructure of CBZ, and altogether four distinct regions (phases) are identified. The EDS spot analysis reveals that the most abundant phase (appearing moderately bright) is $NiAl_3$ containing 74 ± 2 at.% Al and 25 ± 1 at.% Ni (mean $\pm$ standard deviation value based on the data of 10 spots). The phase with bright appearance mainly consists of Cu, Ni, and Al, and its composition closely matches with Al_7Cu_4Ni (58 ± 2 at.% Al, 33 ± 3 at.% Cu, and 9 ± 1 at.% Ni). Besides, there exists α (aluminum-based solid solution containing 0.6 ± 0.1 wt.% Ni and 1.3 ± 0.2 wt.% Cu as alloying elements) and SiC particles with relatively dull appearance. The SiC particles are not segregated (agglomerated) at CBZ because of the presence of Ni in the interlayer. This is in contrast to the SiC particle segregation observed when pure Cu interlayer is used in TLP

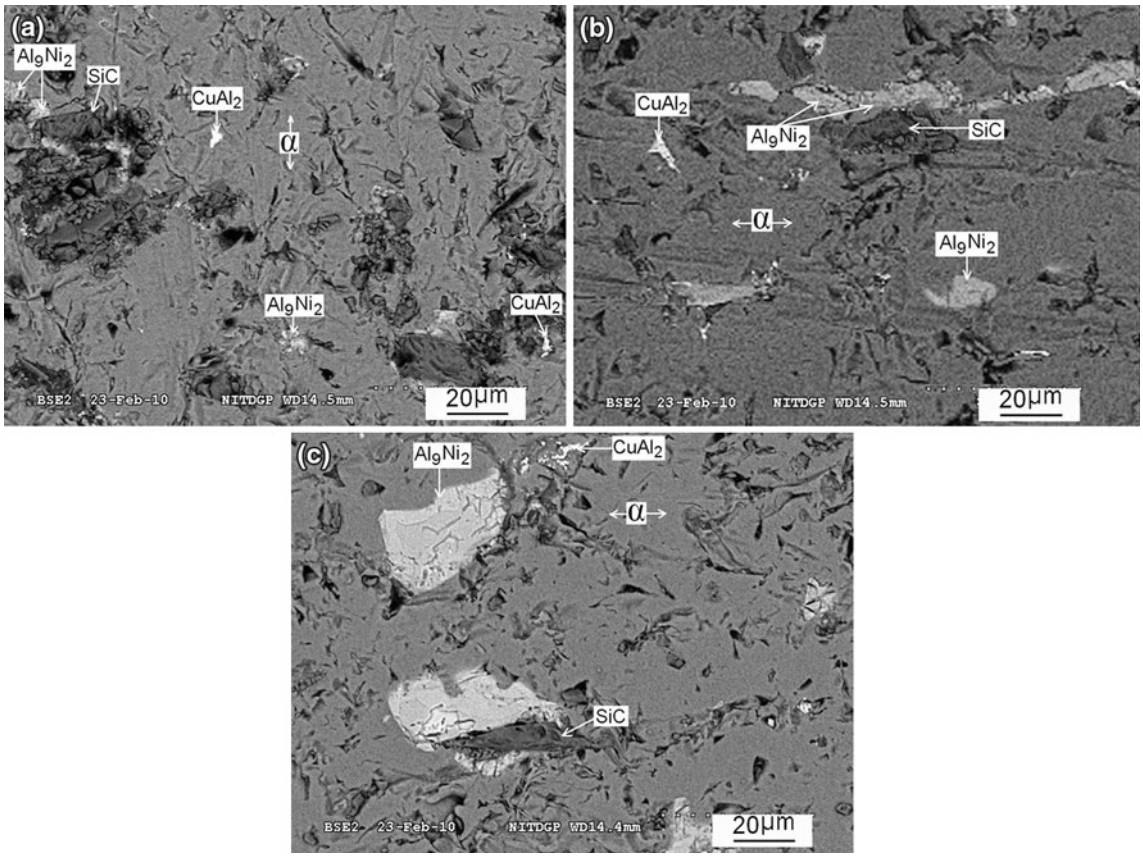

Fig. 8 Back-scattered electron images of the polished and etched section representing isothermally solidified zone for different holding times: (a) 40 min, (b) 2 h, and (c) 6 h

diffusion bonding of the Al/SiCp composites (Ref 28, 29). In case of pure Cu interlayer, complete melting of the interlayer occurs, and during isothermal solidification, the advancing solidification front pushes the SiC particles to cause segregation (Ref 29, 35). However, in the present study, owing to the presence of Ni (element of high melting point), the melting of interlayer (mixed Cu-Ni powder) remains incomplete (particularly in the Ni-enriched CBZ) and the viscosity of Al-Cu-Ni melt is likely to be higher than that of Al-Cu melt. The insoluble particles (SiC) are pushed if the velocity of the solidification front remains below a critical velocity (V_C). The V_C is inversely related to the melt viscosity (Ref 35). Therefore, for Al-Cu-Ni melt, the V_C is relatively lower and the particle segregation is avoided as the solidification front velocity often exceeds V_C. Other than this, microporosities with dark appearance are also visible in CBZ. This is expected, especially at lower bonding time, since the powder interlayer is usually porous and the microstructure that evolves by virtue of the transient diffusion through this porous mass involving incomplete melting of the interlayer is likely to contain microporosity. The specimen with 1-h holding (Fig. 5b) also possesses a heterogeneous microstructure similar to that with 40-min holding. However, as the holding time is increased, with continual diffusion the structural heterogeneity is gradually diminished and the $NiAl_3$ phase (moderately bright in appearance) grows to occupy almost the entire microstructure (Fig. 5c-e). Also, with prolonged holding at the bonding temperature, microporosities are gradually eliminated at CBZ. The result of point count analysis of CBZ representing the relative presence of different micro-constituents for different bonding time is presented in Table 2. It is found that initially CBZ contains about 63% $NiAl_3$, 16% α-solid solution, 10% Al_7Cu_4Ni, 2% SiC, and 9% microporosity. As holding time increases, the proportion of $NiAl_3$ increases; on the other hand, Al_7Cu_4Ni phase and porosities are gradually eliminated. After 6-h holding, the microstructure of CBZ contains mainly the $NiAl_3$ phase (88%) along with a small proportion of α-solid solution (10%), and SiC particles without any visible microporosity (Fig. 5e). The elemental distribution in CBZ for a bonding time of 6 h (corresponding to Fig. 5e) is shown in Fig. 6. This confirms the presence of Al and Ni as the main elements in CBZ.

At the bonding temperature of 560 °C and less, the following invariant and monovariant reactions occur in Al-Cu-Ni ternary system (Ref 36):

Invariant reaction (at 546 °C): Liquid → α + $CuAl_2$ + Al_7Cu_4Ni

Monovariant reaction (between 590 and 546 °C): Liquid → α + Al_7Cu_4Ni

Monovariant reaction (between 547 and 546 °C): Liquid → α + $CuAl_2$

The Al-Cu-Ni ternary phase diagram (Ref 36) representing the stable equilibrium phases at room temperature is shown in Fig. 7. It is found that the $NiAl_3$ phase is stable in a wide range of compositions. Therefore, as holding time increases, the progressive diffusion causes the $NiAl_3$ phase to grow in the

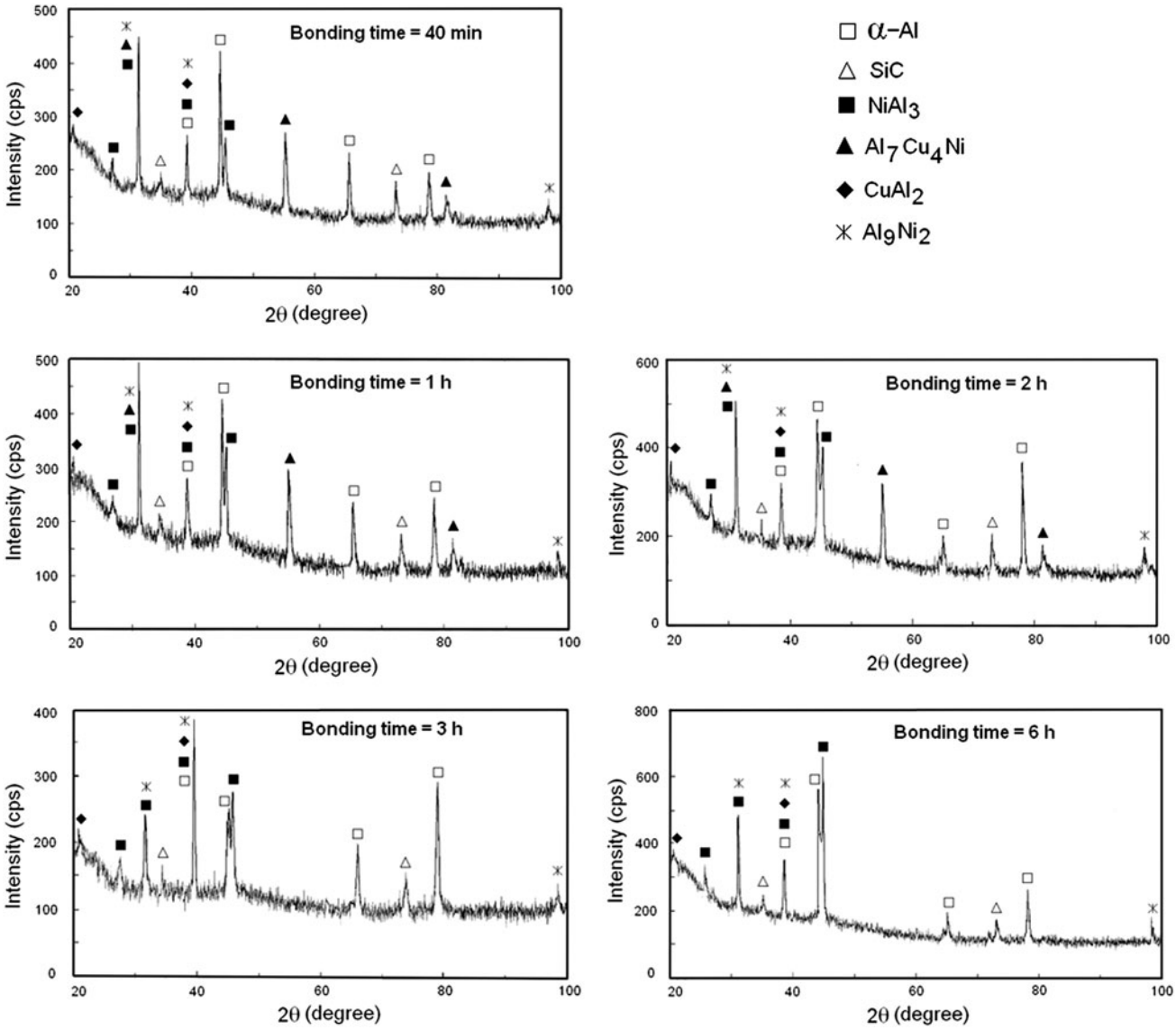

Fig. 9 Result of XRD study

Table 3 Result of shear test

Specimen condition	Bonding time	Shear strength, MPa (mean ± standard deviation)
As-received composite	Not applicable	105 ± 2
Bonded composite	40 min	48 ± 4
	1 h	51 ± 5
	2 h	63 ± 5
	3 h	72 ± 6
	6 h	88 ± 5

microstructure of CBZ eliminating heterogeneity. Moreover, the $NiAl_3$ phase has been reported to exhibit substantial growth on isothermal holding (Ref 37). On the other hand, the Al_7Cu_4Ni phase, though existing in the CBZ at lower bonding time, disappears after holding for a longer time (6 h) as Cu diffuses at a faster rate from CBZ to ISZ. Besides, the diffusion-assisted growth of $NiAl_3$ seals the microporosities.

The typical back-scattered electron images of the ISZ at higher magnification are presented in Fig. 8a-c. The microstructure in all the bonding conditions exhibit the presence of α-solid solution matrix (the most abundant phase), Al_9Ni_2, $CuAl_2$, and SiC particles. The $CuAl_2$ phase (33 ± 2 at.% Cu, and 66 ± 3 at.% Al) appears bright; on the other hand, Al_9Ni_2 (82 ± 4 at.% Al, and 18 ± 1 at.% Ni) is of relatively low brightness. The precipitation of non-equilibrium (metastable) phase Al_9Ni_2 from dilute solution of Al containing Ni has been reported (Ref 38). In the present study, owing to limited diffusion of Ni, the α-solid solution in the ISZ remains diluted with Ni and, accordingly, the metastable Al_9Ni_2 precipitate evolves along with the equilibrium precipitate $CuAl_2$.

The result of XRD study (Fig. 9) adequately supports the phase identification by EDS technique. The thin specimen machined out from the bond region for XRD test includes both the CBZ and ISZ. Therefore, all the phases ($NiAl_3$, α-solid solution, Al_7Cu_4Ni, $CuAl_2$, Al_9Ni_2, and SiC) identified by EDS analysis are also indicated in the XRD pattern. In concurrence

with the SEM observations (Fig. 5a-e; Table 2) the Al_7Cu_4Ni phase is visible up to a holding time of 2 h.

3.2 Bond Strength and Fractured Surface

The shear strength of the joint (bond strength) for various bonding time is presented in Table 3. Typical load-displacement plots are presented in Fig. 10. At lower bonding times (40 min and 1 h), the bond strength is very low. However, as the time of holding increases, the bond strength is improved. The highest joint strength (88 MPa) of the bonded composite is achieved with 6-h holding, which is 84% of the shear strength (105 MPa) of the as-received composite (representing 84% joint efficiency). The typical back-scattered electron images of the fractured surface are shown in Fig. 11a-d. The failure of all the specimens occurs through CBZ. At lower bonding time, the fractured surface exhibits the presence of cracks. It is clearly observed that up to 3-h holding (Fig. 11a-c), the crack originates from microporosities. This is quite probable since microporosities act as the local sites of stress raiser. After being originated at microporosity, the crack propagates through interphase interfaces owing to structural heterogeneity, particularly for lower bonding time. The Al_7Cu_4Ni phase (appearing bright) is so often observed in the vicinity of crack propagation path (Fig. 11a and b). Therefore, the poor bond strength for lower time of holding is attributed to the structural heterogeneity (particularly the presence of Al_7Cu_4Ni) and microporosity. On the other hand, the fractured surface of the specimen with 6-h holding (Fig. 11d) exhibits the presence of naked SiC particle, and no porosity or crack is apparently visible. This indicates that, in the absence of microporosity (crack initiation site), the failure occurs through decohesion at the matrix-particle interface. The elimination of microporosity and development of homogeneity in the microstructure with prolonged holding results in higher joint efficiency.

The joint efficiency (84%) achieved in the present study with mixed Cu-Ni powder interlayer is much higher than the joint efficiency achieved (68%) by Yan et al. (Ref 13) in joining AlMMC using a composite Cu/Ni/Cu foil interlayer. In case of composite foil interlayer, since Cu and Ni were present as separate layers their intermixing through diffusion remained incomplete. This resulted in highly heterogeneous microstructure with several interphase interfaces. As a consequence, the failure process was accentuated where crack originated and propagated in the vicinity of a non-equilibrium phase, reported as $Al_{0.9}$ $Ni_{1.1}$, thereby lowering the joint efficiency (Ref 13). In the present investigation, a thoroughly mixed Cu and Ni powders are used as the interlayer. Therefore, after 6-h holding, more homogeneous structure is achieved with negligible porosity owing to continual diffusion. This results in a better joint efficiency. However, still higher joint efficiency (89-90%) was achieved by the present authors (Ref 39, 40) while joining the same composite at 560 °C under 0.2-MPa pressure with 6-h holding time using 50-μm-thick pure copper interlayer (in foil or powder form). A critical analysis of bonding with copper interlayer (where interlayer undergoes complete melting) explored that during isothermal solidification, though the SiC particles are pushed by the solid/liquid interface to cause segregation, the liquid-particle aggregate simultaneously moves toward the periphery (edge) of the cross section to gradually remove the effect of segregation (Ref 41). Therefore, particle segregation persisted only for shorter holding time (up to about 2 h) in concurrence with that suggested by previous investigators (Ref 28, 29). However, for longer holding time, the particle segregation was eliminated and the microstructure at the joint region predominantly consisted of α-solid solution (aluminum-based solid solution) and uniformly distributed SiC particles. Such a microstructure provided higher joint efficiency (89-90%) than the present study (84%) where, after 6-h holding, the microstructure at the central bond region mainly consists of $NiAl_3$ along with a few SiC particles. The relatively lower joint efficiency in the present study is attributed to the presence of more brittle intermetallic phase $NiAl_3$ (as compared to α-solid solution of previous study) that is reflected in the flat, fractured surface (Fig. 11d). Therefore, the effectiveness of using Cu-Ni mixed powder interlayer is limited to a joint efficiency of 84%. The use of copper interlayer is relatively more effective with judicious selection of bonding parameters.

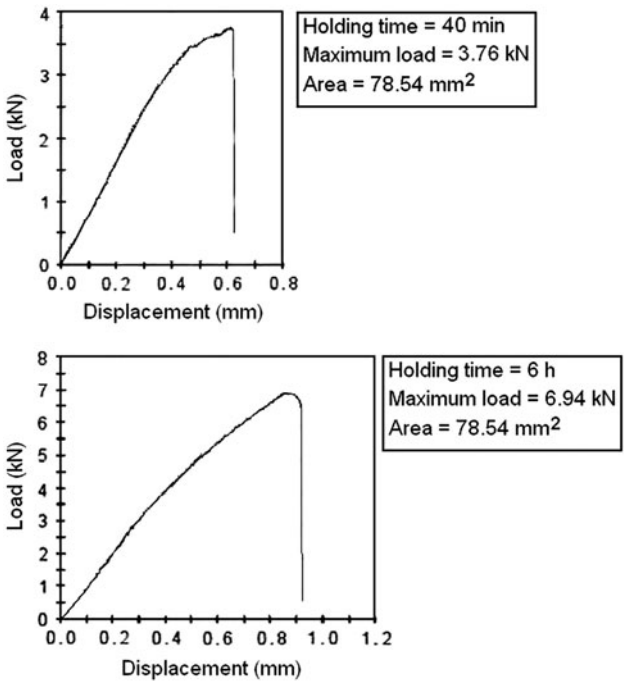

Fig.10 Typical load-displacement plots of tensile shear test

4. Conclusion

(i) In the TLP-phase diffusion bonding of 6061-15 wt.% SiCp composite at 560 °C, 0.2 MPa, using mixed Cu-Ni powder interlayer, the bond region mainly consists of two zones, namely, (a) the central bond zone, and (b) the isothermally solidified zone.

(ii) The microstructure of the isothermally solidified zone contains equilibrium precipitate $CuAl_2$, and the metastable precipitate Al_9Ni_2 in the matrix of α-solid solution along with the reinforcement particles (SiC).

(iii) The microstructure of the central bond zone is highly heterogeneous at the lower bonding time. The equilibrium phases, such as $NiAl_3$, Al_7Cu_4Ni, and α-solid solution along with the reinforcement particle (SiC), are found to be present. Unlike the bonding with pure Cu interlayer, segregation of SiC particles is avoided. However, the microporosities are observed.

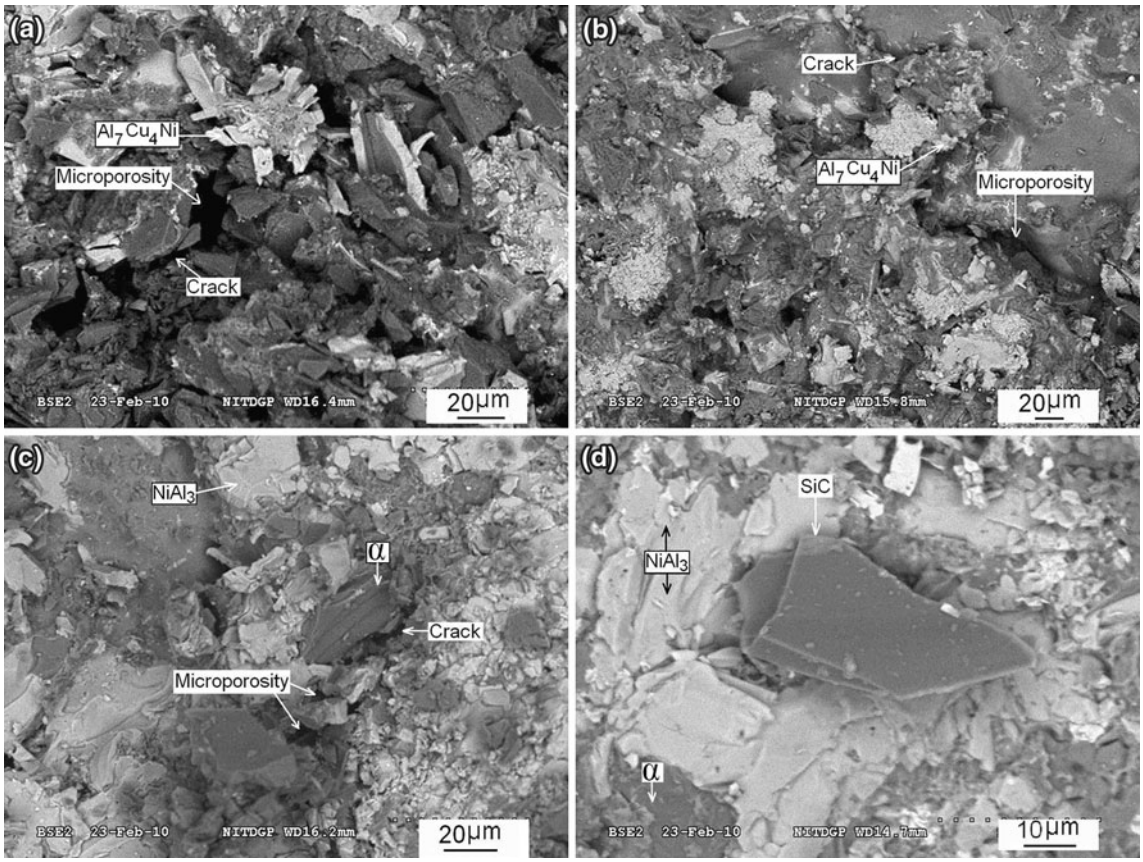

Fig. 11 Back-scattered electron images of the fractured surfaces of bonded composites: (a) 40 min, (b) 2 h, (c) 3 h, and (d) 6 h

(iv) As the bonding time increases, owing to continual diffusion, $NiAl_3$ phase grows, the structural heterogeneity is gradually diminished with disappearance of Al_7Cu_4Ni phase, and the microporosities are eliminated at the central bond zone. After 6-h holding, the microstructure of the central bond zone mainly consists of $NiAl_3$ without any visible microporosity.

(v) At lower holding time, during shear test, the crack originates from microporosities and propagates along interphase interfaces (mainly in the vicinity of Al_7Cu_4Ni phase) resulting in poor bond strength. However, the specimen with 6 h of holding, owing to structural homogeneity (nonexistence of Al_7Cu_4Ni) and absence of porosity, exhibits the highest bond strength where the failure primarily occurs through the decohesion at the SiC particle/matrix interface. The achieved joint efficiency (84%) in the present study with mixed Cu-Ni powder interlayer is much higher than that (68%) achieved with composite Cu/Ni/Cu foil interlayer. However, it is still lower than that obtained with pure copper interlayer.

Acknowledgment

The authors acknowledge the support of several undergraduate students, including Saswata Banerjee, Imran Ahmed, and Subrata Das of the Metallurgical and Materials Engineering Department in various occasions, and the operational assistance in Scanning Electron Microscopy provided by Somnath Ghatak of the Central Instrumental Facility, the National Institute of Technology, Durgapur, India. The authors are also grateful to the Director, the National Institute of Technology, Durgapur, India, for providing the necessary financial and administrative support.

References

1. D. Huda, M.A.El Baradie, and M.S.J. Hashmi, Metal-Matrix Composites: Materials Aspects, Part II, *J. Mater. Process. Technol.*, 1993, **37**, p 529–541
2. T.J. Lienert, W.A. Baeslack, J. Ringnalda, and H.L. Fraser, Inertia-Friction Welding of SiC-Reinforced 8009-Aluminium, *J. Mater. Sci.*, 1996, **31**, p 2149–2157
3. M.B.D. Ellis, Joining of Metal Matrix Composites—A Review, *TWI, J.*, 1997, **6**, p 69–128
4. W.I. Hall and F. Manrique, Surface Treatment of Carbon Fiber for Aluminium Alloy Matrix Composites, *Scr. Met.*, 1995, **33**, p 2037–2043
5. M.F. Gittos and P.L. Threadgill, Preliminary Studies of joining particulate reinforced Aluminium Alloy Metal Matrix Composites', *Proceedings of International Symposium on* '*Metal Matrix Composites III: Exploiting the Investment*', Dec. 10–11, 1991, Institute of Metals, London
6. T.S. Luhman, R.L. Williams, and K.B. Das, Development of Joint and Joining Techniques for Metal Matrix Composites, *Fourth Quarterly Progress Report*, Army Materials and Mechanics Research Center, 1983, p 1–58
7. J.H. Devletian, SiC/Al Metal Matrix Composite Welding by a Capacitor Discharge Process, *Weld. J.*, 1987, **66**, p 33–39
8. D.J. Field, *Aluminium Alloys—Contemporary Research and Applications*, Vol 31, London Academic Press, London, 1989, p 523–537
9. A. Urena, J.M. Gomez de Salazar, and M.D. Escalera, Diffusion Bonding of Discontinuously Reinforced SiCp/Al Matrix Composites, *Key Eng. Mater.*, 1995, **104–107**, p 523–540
10. A.A. Shirzadi and E.R. Wallach, New Approaches for Transient Liquid Phase Diffusion Bonding of Aluminium Based Metal Matrix Composites, *Mater. Sci. Technol.*, 1997, **13**, p 135–142

11. J. Huang, Y. Dong, Y. Wan, X. Zhao, and H. Zhang, Investigation on Reactive Diffusion Bonding of SiCp/6063 MMC by Using Mixed Powders as Interlayers, *J. Mater. Process. Technol.*, 2007, **190**, p 312–316
12. T.K. Pal, Joining of Aluminium Metal Matrix Composites, *Mater. Manuf. Process.*, 2005, **20**, p 717–726
13. J. Yan, Z. Xu, G. Wu, and S. Yang, Interface Structure and Mechanical Performance of TLP Bonded Joints of Al_2O_3p/6061 Al Composites Using Cu/Ni Composite Interlayers, *Scr. Mater.*, 2004, **51**, p 147–150
14. D.S. Duvall, W.A. Owczarski, and D.F. Paulonis, TLP Bonding: A New Method for Joining Heat Resistant Alloys, *Weld. J.*, 1974, **53**, p 203–214
15. I. Tuah-Poku, M. Dollar, and T.B. Massalski, A Study of the Transient Liquid Phase Bonding Process Applied to a Ag/Cu/Ag Sandwich Joint, *Metall. Trans. A*, 1988, **19A**, p 675–686
16. Y. Natsume, K. Ohsasa, Y. Tayu, T. Momono, and T. Narita, Numerical Modeling of Transient Liquid-Phase Diffusion Bonding Process of Al using Cu Filler Metal, *ISIJ Int.*, 2003, **43**, p 1976–1982
17. D.F. Paulonis, D.S. Duvall, and W.A. Owczarski, US Patent 3,678,570, 1972
18. A.T. Egbewande, C. Chukwukaeme, and O.A. Ojo, Joining of Superalloy Inconel 600 by Diffusion Induced Isothermal Solidification of a Liquated Insert Metal, *Mater. Charact.*, 2007, **59**, p 1051–1058
19. N.P. Wikstrom, O.A. Ojo, and M.C. Chaturvedi, Influence of Process Parameters on Microstructure of Transient Liquid Phase Bonded Inconel 738LC Superalloy with Amdry DF-3 Interlayer, *Mater. Sci. Eng. A*, 2006, **417**, p 299–306
20. D.Q. Sun, W.H. Liu, and X.Y. Gu, Transient Liquid Phase Bonding of Magnesium alloy (Mg-3Al-1Zn) Using Copper Interlayer, *Mater. Sci. Technol.*, 2004, **20**, p 1595–1598
21. T. Padron, T.I. Khan, and M.J. Kabir, Modelling the Transient Liquid Phase Bonding Behaviour of a Duplex Stainless Steel Using Copper Interlayers, *Mater. Sci. Eng. A*, 2004, **385**, p 220–228
22. T.I. Khan, M.J. Kabir, and R. Bulpett, Effect of Transient Liquid-Phase Bonding Variables on the Properties of Micro-Duplex Stainless Steel, *Mater. Sci. Eng. A*, 2004, **372**, p 290–295
23. W.F. Gale, D.A. Butts, M.D. Ruscio, and T. Zhou, Microstructure and Mechanical Properties of Titanium Aluminide Wide-Gap, Transient Liquid-Phase Bonds Prepared Using a Slurry-Deposited Composite Interlayer, *Metall. Mater. Trans. A*, 2002, **33A**, p 3205–3214
24. T.I. Khan and B.N. Roy, Transient Liquid Phase Bonding of an ODS Ferrite Steel to Silicon Nitride, *J. Mater. Sci.*, 2004, **39**, p 741–743
25. R.S. Bushby and V.D. Scott, Liquid Phase Bonding of Aluminium and Aluminium/Nicalon Composite Using Copper Interlayers, *Mater. Sci. Technol.*, 1993, **9**, p 417–423
26. R.S. Bushby and V.D. Scott, Liquid Phase Bonding of Aluminium and Aluminium/Nicalon Composite Using Interlayers of Cu-Ag Alloy, *Mater. Sci. Technol.*, 1995, **11**, p 643–649
27. R. Klen and T.W. Eagar, Joining of 6061 Aluminium Metal-Ceramic Particle Reinforced Composites, *WRC Bull.*, 1993, **385**, p 1–26
28. Z. Li, Y. Zhou, and T.H. North, Counteraction of Particulate Segregation During Transient Liquid-Phase Bonding of Aluminium-Based MMC Material, *J. Mater. Sci.*, 1995, **30**, p 1075–1082
29. J. Maity, T.K. Pal, and R. Maiti, Microstructural Evaluation and Ultrasonic Characterization of TLPD Bonded 6061-SiCp Composite, *ISIJ int.*, 2008, **48**, p 616–623
30. J.R. Askew, J.F. Wilde, and T.I. Khan, Transient Liquid Phase Bonding of 2124 Aluminium Metal Matrix Composite, *Mater. Sci. Technol.*, 1998, **14**, p 920–924
31. Anon, Properties and Selection: Non Ferrous Alloys and Special Purpose Materials, Vol 2, *Metals Handbook*, 10th ed., ASM International, Metals Park, OH, 1990, p 102–103
32. Anon, Alloy Phase Diagrams, Vol 3, *ASM Handbook*, ASM International, Metals Park, OH, 1992, p 2.44–3.10
33. M. Jain and S.P. Gupta, Formation of Intermetallic Compounds in the Ni-Al-Si Ternary System, *Mater. Charact.*, 2003, **51**, p 243–257
34. V. Raghavan, Al-Cu-Ni (Aluminium-Copper-Nickel), *J. Phase Equilib. Diffus.*, 2006, **27**, p 389–391
35. D. Shangguan, S. Ahuja, and D.M. Stefanescu, An Analytical Model for the Interaction Between an Insoluble Particle and an Advancing Solid/Liquid Interface, *Metall. Trans. A*, 1992, **23A**, p 669–680
36. N.A. Belov, D.G. Eskin, and A.A. Aksenov, *Multicomponent Phase Diagrams: Applications for Commercial Aluminium Alloys*, 1st ed., Elsevier, Oxford, 2005, p 227–229
37. X.A. Zhao, E. Ma, and M.A. Nicolet, Growth Kinetics of $NiAl_3$ Formation on Large-Grained <Al> Substrates, *Mater. Lett.*, 1987, **5**, p 200–202
38. A. Yamamoto and H. Tsubakino, Al_9Ni_2 Precipitates Formed in an Al-Ni Dilute Alloy, *Scr. Mater.*, 1997, **37**, p 1721–1725
39. J. Maity, T.K. Pal, and R. Maiti, Transient Liquid Phase Diffusion Bonding of 6061-15 wt.% SiCp in Argon Environment, *J. Mater. Process. Technol.*, 2009, **209**, p 3568–3580
40. J. Maity, T.K. Pal, and R. Maiti, Transient Liquid Phase Bonding of 6061-15 wt.% SiCp in Argon Environment Using Cu Powder Interlayer, *Mater. Sci. Technol.*, 2009, **25**, p 1489–1494
41. J. Maity, T.K. Pal, and R. Maiti, Transient Liquid-Phase Diffusion Bonding of 6061-13 vol.% SiCp Composite Using Cu Powder Interlayer: Mechanism and Interface Characterization, *J. Mater. Sci.*, 2010, **45**, p 3575–3587